NANO LETTERS

Letter

pubs.acs.org/NanoLett

Looking into Meta-Atoms of Plasmonic Nanowire Metamaterial

Kun-Tong Tsai,[†,‡,§] Gregory A. Wurtz,[§] Jen-You Chu,[∥] Tian-You Cheng,[⊥] Huai-Hsien Wang,[‡] Alexey V. Krasavin,[§] Jr-Hau He,[*,†,¶] Brian M. Wells,[#] Viktor A. Podolskiy,[#] Juen-Kai Wang,[*,‡,⊥] Yuh-Lin Wang,[*,‡,∇] and Anatoly V. Zayats[*,§]

[†]Graduate Institute of Photonics and Optoelectronics and Department of Electrical Engineering, National Taiwan University, Taipei 10617, Taiwan

[‡]Institute of Atomic and Molecular Sciences, Academia Sinica, Taipei 10617, Taiwan

[§]Department of Physics, King's College London, Strand, London WC2R 2LS, U.K.

[∥]Material and Chemical Research Laboratories, Industrial Technology Research Institute, Hsin-Chu 31040, Taiwan

[⊥]Center for Condensed Matter Sciences, National Taiwan University, Taipei 10617, Taiwan

[#]Department of Physics and Applied Physics, University of Massachusetts Lowell, Lowell, Massachusetts 01854, United States

[∇]Department of Physics, National Taiwan University, Taipei 10617, Taiwan

[¶]Computer, Electrical and Mathematical Sciences and Engineering Division, King Abdullah University of Science & Technology, Thuwal 23955-6900, Saudi Arabia

Supporting Information

ABSTRACT: Nanowire-based plasmonic metamaterials exhibit many intriguing properties related to the hyperbolic dispersion, negative refraction, epsilon-near-zero behavior, strong Purcell effect, and nonlinearities. We have experimentally and numerically studied the electromagnetic modes of individual nanowires (meta-atoms) forming the metamaterial. High-resolution, scattering-type near-field optical microscopy has been used to visualize the intensity and phase of the modes. Numerical and analytical modeling of the mode structure is in agreement with the experimental observations and indicates the presence of the nonlocal response associated with cylindrical surface plasmons of nanowires.

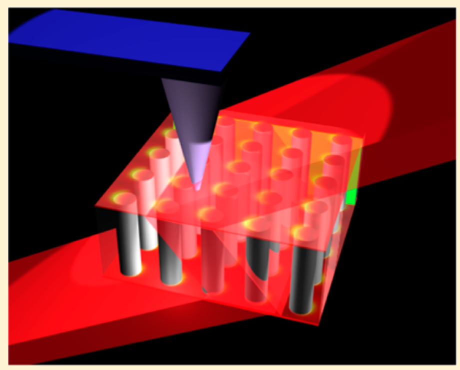

KEYWORDS: *Metamaterials, plasmonics, nanowires, SNOM, nonlocality, epsilon-near-zero*

Metamaterials enable unprecedented control over light propagation[1,2] and enhanced light−matter interactions at the nanoscale,[3−6] opening new avenues for the applications beyond the scope covered by natural materials. One of the practical metamaterial designs is based on the constituent meta-atoms in the form of aligned metal wires placed in the embedding dielectric with both wire diameter and interwire separation much smaller than the wavelength of light at the operating frequency. Such wire metamaterials[7] are of special interest due to their unusual anisotropic optical properties manifested in hyperbolic dispersion,[8,9] optical nonlocality effects,[10,11] and extreme field confinement[12] important for numerous applications in imaging,[2,13−16] active nanophotonics,[11,17,18] and bio/chemo-sensing.[19] Since the metamaterial structure is relatively simple, the barrier associated with the fabrication difficulties is greatly reduced compared to top-down fabricated metamaterials based on, e.g., split-ring resonators or fishnets,[20,21] and scaling down to optical operational frequencies is relatively easy.[7] Therefore, these metamaterials enable operating frequencies spanning a very broad range from infrared to visible and, possibly, to the ultraviolet wavelength range.

For wire metamaterials operating at optical frequencies, namely, near-infrared and visible, constituent elements are usually plasmonic nanowires of relatively short length (also called nanorods) to achieve resonances in the desired wavelength range. The behavior of these optically dense arrays of nanowires embedded in dielectric matrices can be conceptually described using an effective medium approximation, introducing the anisotropic effective permittivity tensor of the metal−dielectric composite. In such metamaterials, the components of the permittivity tensor along and perpendicular to the nanowire axis may have opposite signs resulting in the hyperbolic isofrequency surfaces of the dispersion.[8] The hyperbolic dispersion enables the broadband negative refraction[2,13] and controllable spontaneous emission[4] in the

Received: April 7, 2014
Revised: July 29, 2014
Published: August 12, 2014

nanowire metamaterials. Other applications, such as subwavelength color imaging,[12] sensing,[22] and designed ultrafast optical nonlinearity,[11] are also of significant interest.

Although the optical properties of plasmonic nanorod and nanowire metamaterials have been extensively studied, the observations are generally limited to far-field measurements reflecting the effective medium behavior of the metamaterial. At the same time, microscopic phenomena related to the internal structure of the composite, accessible in the near-field region of the metamaterial where its structure is important, have been inferred only numerically via simulations of microscopic field distributions. The direct observation of the local field distribution down to the meta-atom scale in the nanowire metamaterial at optical frequency has not been characterized experimentally, inhibiting fundamental understanding of electromagnetic phenomena within the metamaterial, including Purcell and nonlocal effects, for which the internal metamaterial structure is of great importance.[23]

The experimental demonstration of the optical signatures of individual nanowires within the array structure remains a major challenge due to the limited spatial resolution of optical microscopy. Recently, the development of scattering-type (also called apertureless) scanning near-field optical microscopy (s-SNOM)[24−26] allows one to reveal the optical details at the deep subwavelength scales and has already provided insight into electromagnetic (EM) waves interaction with composite metamaterials.[27−32] Complementary far-field and near-field optical studies are required to gain a rational understanding of the character of the underlying mechanisms of light interaction with metamaterials on the nanoscale, providing the opportunity for a controlled improvement of new metamaterial designs.

In this letter, we report on the first experimental observation of near-field behavior of nanowire metamaterials on the meta-atom scale at visible frequencies. The optical mode within the unit cell less than 100 nm is visualized utilizing s-SNOM. The results are consistent with numerical simulations confirming the near-field signature of individual meta-atoms in the nanowire metamaterials. We show that the near-field behavior of meta-atoms in metamaterial is similar to the behavior of an isolated nanorod, determined by the excitation of cylindrical surface plasmons, while the far-field response is dominated by coupling between the meta-atoms.

The nanowire metamaterial studied in this work (Figure 1) is made of vertically aligned silver nanowires (AgNWs) embedded in an anodic aluminum oxide (AAO) matrix (Figure 1a). The fabrication of the nanowire metamaterial has been described in detail elsewhere[14] (also see Supporting Information). In brief, the nanowire metamaterial is fabricated by performing an electrochemical deposition of silver into the empty pores of the AAO templates. AAO templates are made with the arrays of highly ordered nanochannels, and a mechanical chemical polish process is carried out to ensure its flatness, which allows the geometries in the experiment to be compared to simulations. The diameter and length of the nanowires are of about 50 nm and 5 μm, respectively. They are arranged in an array with a hexagonal close-packed (hcp) lattice of about 100 nm period. The atomic force microscope (AFM) topography image (Figure 1b) shows the sample's flatness with a root-mean-square roughness as small as 3.5 nm.

The effective permittivity of the metamaterial (Figure 1c) deduced using the Maxwell−Garnet effective medium approximation[33] shows that the hyperbolic regime occurs for the

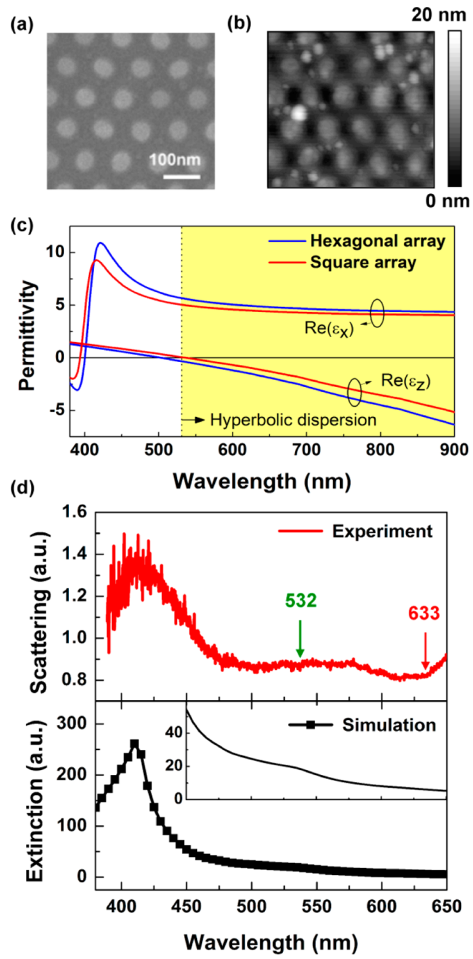

Figure 1. (a) Scanning electron microscope and (b) atomic force microscope topography images, and (c) effective permittivities (real parts) of the nanowire metamaterials. (d) Measured dark-field scattering spectrum and the simulated extinction spectrum for the nanowire metamaterial. The arrows indicate the laser lines used in the s-SNOM measurements. The simulated extinction spectrum is obtained at the incident angle of 60°, which corresponds to the illumination condition in the s-SNOM experiment.

wavelengths longer than around 530 nm. The measured scattering spectrum and the extinction spectrum calculated using the finite-element simulations (see Methods in Supporting Information for details) are shown in Figure 1d. The scattering spectrum has a dominant peak at the wavelength of about 415 nm, which is the transverse mode of the AgNWs, related to the resonant electron oscillations perpendicular to the nanowire axes.[34] At this resonant peak, strong scattering and high absorption occur. We focus on the optical properties away from this resonance where the absorption is relatively low. The wavelengths of 532 and 633 nm, used in the near-field measurements, are away from high absorption and close to the epsilon-near-zero (ENZ) condition and in the hyperbolic dispersion range, respectively.

To map the near-field distribution over the nanowire metamaterials, an amplitude- and phase-resolved scattering-type scanning near-field optical microscope (s-SNOM) has been used (Figure S3, Supporting Information).[24] An objective lens focuses a TM-polarized laser beam onto the AFM tip at an incident angle of 60°. A Pt−Ir-coated Si cantilever was used in the experiments since its plasmonic resonance is away from the

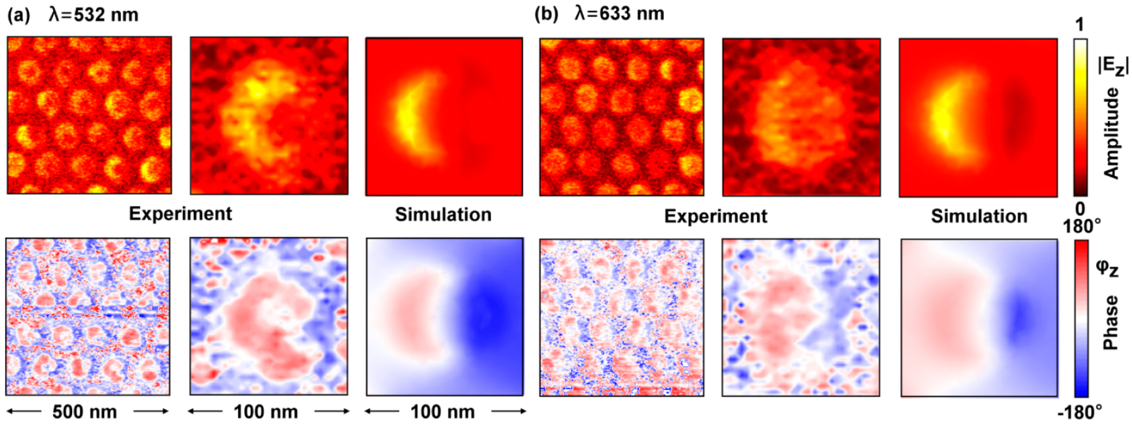

Figure 2. Measured and simulated near-field distributions of the electric-field (z-component) and phase above the nanowire metamaterials at the wavelengths of (a) 532 and (b) 633 nm. The simulated distributions are presented at the height of 5 nm above the nanowire metamaterial's surface. The illumination of the metamaterial is from the right at 60° angle of incidence.

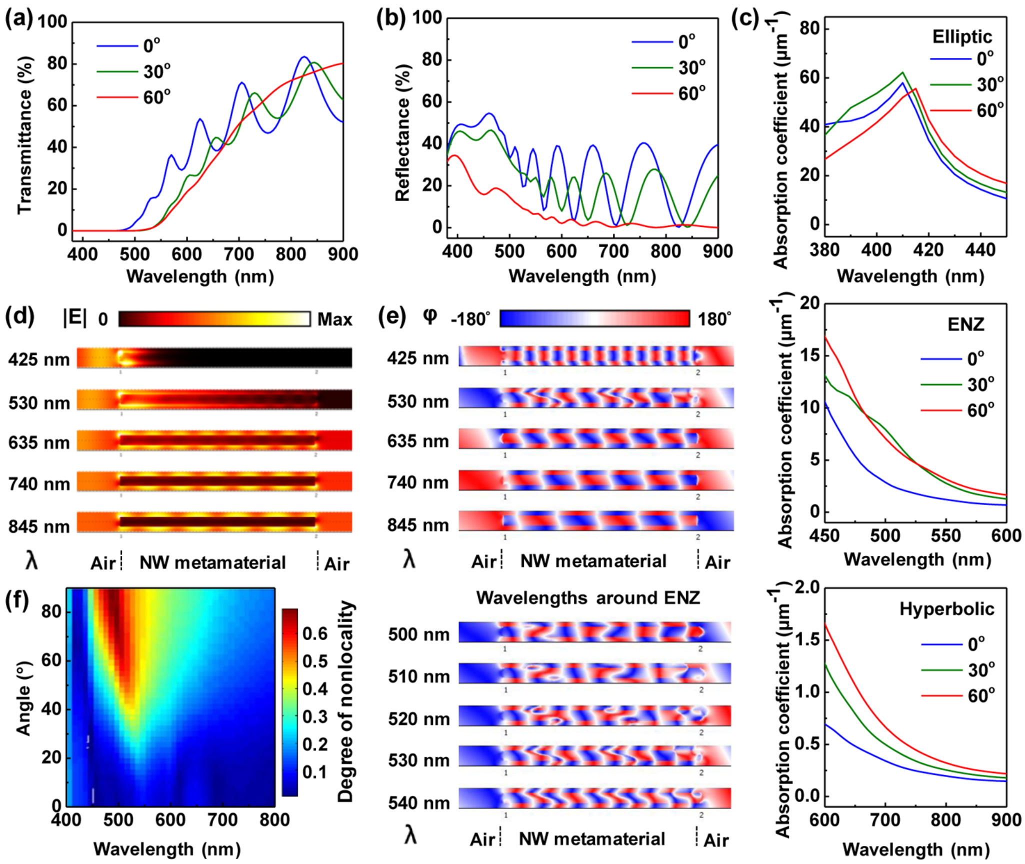

Figure 3. Simulated (a) transmittance, (b) reflectance, and (c) absorption coefficient spectra of the nanowire metamaterial at the incident angles of 0°, 30°, and 60°. (d) The electric field distributions (|*E*|) and (e) phase distributions (φ) for different wavelengths at the incident angle of 30°. (f) The amplitude contribution of the additional TM wave, calculated using a nonlocal EMT theory[36] for different wavelengths and angles of incidence. The metamaterial consists of 1 μm long silver nanowires, all other parameters as in Figure 2.

laser wavelengths used in this study and relatively wavelength insensitive, therefore preventing the introduction of unwanted near-field electromagnetic interactions from the tip apex. A heterodyne interferometric setup has been employed to extract the amplitude and phase of the electromagnetic field near the metamaterial surface. In order to remove the background of the far-field scattered light, the optical signal modulated at the fourth harmonic of the tip vibration was monitored.[25] The resolution of the s-SNOM setup was typically sub-10 nm and therefore adequate to detect the details of near-field information on the nanowire metamaterials with the metamaterial unit cell less than 100 nm.

The measured and calculated near-field intensity and phase distributions in the arrays of nanowires are shown in Figure 2a,b for the illumination with the TM polarized light at the wavelengths of 532 and 633 nm, respectively (see Figure S4, Supporting Information, for the images with saturated contrast). The periodic pattern of the near-field intensity

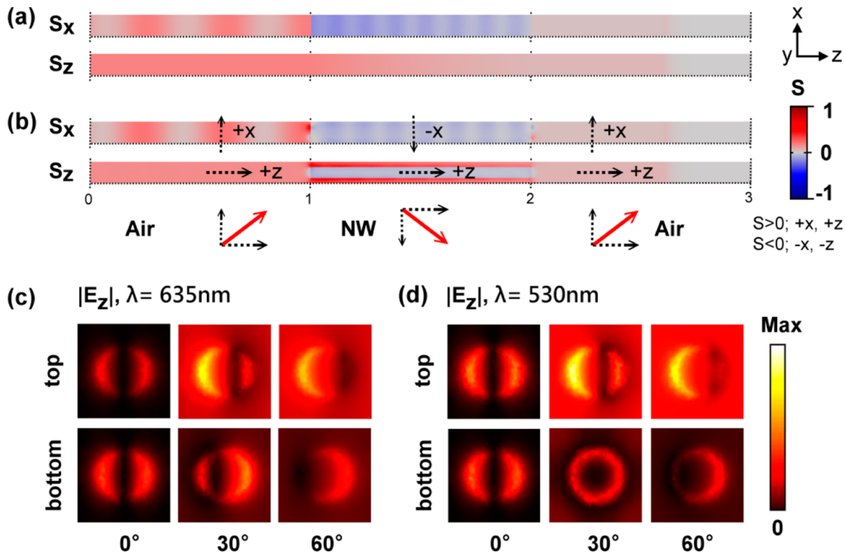

Figure 4. Simulated distribution of the x- and z-components of the time-averaged energy flow for (a) a layer of a homogeneous effective medium and (b) AgNWs/AAO composite (with square lattice) at the wavelength of 635 nm and an incident angle of 30°. The arrows indicate the direction of the energy flow. (c,d) The simulated amplitude distributions of the electric field (z-component) at the wavelengths of 635 and 530 nm, respectively, for different angles of incidence. The field is measured at the height of 5 nm above (below) the top (bottom) metamaterial's surface. The amplitude of $|E_z|$ at the bottom surface in panel d at the incident angles of 30° and 60° is magnified 2.5 and 1.4 times, respectively. The nanowire parameters are the same as those in Figure 3.

reflects the microscopic structure of the metamaterial. The close-up of the near-field distribution around individual meta-atoms forming the metamaterial reveals crescent-shaped distributions around the nanorods for both the intensity and the phase. The symmetry breaking is due to the oblique illumination of the metamaterial from the right at the 60° angle of incidence. The experimental near-field distributions are well reproduced by the map of the z-component of the field only (Figures 2 and S5, Supporting Information); it agrees with the fact that s-SNOM is more sensitive to the field component, which is perpendicular to the sample surface (i.e., $|E_z|$, in our configuration).[24,35] For comparison, the simulation results of the field distribution on the top surface of the metamaterial at the incident angle of 0° is shown in Figure S5b, Supporting Information. The symmetry of the field distribution indicates that the field is built by electron oscillations perpendicular to the nanowire axes. The phase difference at the two ends of the field patterns is around 180°. These properties correspond to the excitation of cylindrical surface plasmons on the nanowires. These charge oscillations are also responsible for nonlocal effects in this system.[36] Over a wide range of wavelengths, the field distributions exhibit similar behavior with the angle of incidence (Figure S5b,c, Supporting Information). It is important to note that the observed field distributions around the nanowires forming metamaterial are similar to those for individual nanowires with a crescent shape for oblique incidence but with different amplitudes in the lobes, indicative of the interaction between the meta-atoms in the metamaterial (Figure S6, Supporting Information). While the near-field behavior of meta-atoms in metamaterial is similar to the behavior of an isolated nanorod, the far-field response is dominated by coupling between the meta-atoms.

The optical properties of the nanowire metamaterials are presented in Figure 3. The absorption is significant over the broad visible spectral range, with the dominating transmission at longer wavelengths (Figure 3a) and reflection at short wavelengths (Figure 3b). The oscillations observed in the spectra are related to the Fabry–Pérot-type resonances due to the reflections of the cylindrical surface plasmons on the metamaterial interfaces. At short-wavelengths (below 450 nm), the absorption due to the transverse resonances of the metamaterial (electron oscillations perpendicular to wire axis) dominates, leading to short penetration depth of light in the metamaterial (Figure 3c). For longer than the ENZ wavelengths, corresponding to the hyberbolic dispersion regime, characteristic field oscillations of the cylindrical surface plasmon interference pattern are observed. The EM waves are mainly confined and propagates along the surface of the Ag NWs. It is interesting to note that, at around the ENZ wavelength (500–540 nm; the ENZ occurs at 537 or 507 nm for the metamaterial with square or hcp lattice, respectively), the intrinsic absorption coefficient of the metamaterial has a peculiarity with increased absorption despite that the local effective parameters behave monotonously. In optically thick materials, nonlocality gives rise to a longitudinal wave that fundamentally changes the optical properties of the system. The two main phenomena associated with the longitudinal wave are illustrated in Figure 3d–f. Coupling of the incident plane wave to the longitudinal wave results in the spectral dependencies of the reflection from and transmission through the metamaterial, which substantially deviate from the predictions of the local effective medium theory for short wavelengths (elliptical dispersion regime) (Figure S7, Supporting Information). Signatures of the interference between the two waves, including vanishing transmission and length-dependent absorption coefficient, are expected in the spectral range where the amplitudes of both waves are comparable to each other (Figure 3f). In both amplitude and especially phase distributions, peculiarities related to interference of two p-polarized waves supported by nonlocal nanowire material are observed around the wavelength of 530 nm (Figure 3d,e).

In order to confirm the negative refraction in the nanowire metamaterial in the hyperbolic regime and to understand the interplay between macroscopic and microscopic behavior, we

dx.doi.org/10.1021/nl501283c | *Nano Lett.* 2014, 14, 4971–4976

investigated the spatial distribution of the time-averaged energy flow through the metamaterial (Figure 4). Figure 4a,b show the simulated *x*- and *z*-components of time-averaged energy flow distributions (i.e., S_x and S_z) for the nanowire metamaterial as a layer of effective medium and the AgNW/AAO composite, respectively. For similar metamaterials, the negative refraction has been experimentally demonstrated.[13] Both effective medium and discrete composite model give the same far-field properties of the metamaterial. In the effective medium scenario (Figure 4a), the sign of S_x flips at the air/metamaterial interface, which indicates an energy flow backward in the lateral direction. At the same time, the S_z homogeneously flows away from the interface. While a similar behavior is observed in the discrete system of nanowires forming the metamaterial, there is a subtle difference between them. In the AgNW/AAO composite, both S_x and S_z show the characteristic near-field signatures of the nanowire geometry (Figure 4b). Further from the nanowire interface, S_x is comparable to the one obtained in the effective medium layer in terms of the power flow distribution.

Figure 4c,d show the simulated angle-dependent amplitude of electric field (*z*-component as measured with a-SNOM) at the wavelength of 635 and 530 nm, corresponding to the hyperbolic dispersion and the ENZ regime, respectively, in the case of square lattice nanowire array. These distributions are practically independent of the type of the lattice, which is expected within validity of the effective medium approximation. At the wavelength of 635 nm, the field distributions at the top and bottom interfaces change with the incident angle, in agreement with the experimental observations. For the wavelength close to the ENZ conditions, a different behavior is observed at 30° angle of incidence, which is related to the nonlocal effects: $|E_z|$ distributed circularly at the bottom surface; at this wavelength−angle combination (Figure 3f), the contribution of the additional wave is significant.

In conclusion, we have experimentally studied the near-field and phase distributions in the composite NW metamaterials using s-SNOM, revealing the response of individual meta-atoms, and numerically simulated their behavior in different regimes of hyperbolic and ENZ dispersions. The near-field measurements reveal collective electronic oscillations (CSPs) of each nanowire, which determine the far-field optical response of the NW metamaterial and are responsible for the nonlocal behavior of the composite.

■ ASSOCIATED CONTENT

Supporting Information

Materials and methods (fabrication of metamaterials, dark-field spectroscopy, finite-element simulations, and scanning near-field optical microscopy). Supplementary Figures. This material is available free of charge via the Internet at http://pubs.acs.org.

■ AUTHOR INFORMATION

Corresponding Authors

*(J.-H.H.) E-mail: jhhe@cc.ee.ntu.edu.tw.
*(J.-K.W.) E-mail: jkwang@ntu.edu.tw.
*(Y.-L.W.) E-mail: ylwang@pub.iams.sinica.edu.tw.
*(A.V.Z.) E-mail: a.zayats@kcl.ac.uk.

Notes

The authors declare no competing financial interest.

■ ACKNOWLEDGMENTS

This work was supported, in part, by the Ministry of Science and Technology of Taiwan (MOST 102-2628-M-001-008 and MOST 102-2112-M-002-011-MY3), US Army Research Office (W911NF-12-1-0533), EPSRC (U.K.), and the ERC iPLASMM project (321268). K.T.T. acknowledges the support from National Science Council of Taiwan via the Graduate Student Study Abroad Program of Taiwan and NanoCore facilities at Academia Sinica. A.Z. acknowledges support from the Royal Society and the Wolfson Foundation. G.W. acknowledges support from the EC FP7 project 304179 (Marie Curie Actions). The authors are grateful to D. O'Connor for help with the numerical model.

■ REFERENCES

(1) Lemoult, F.; Kaina, N.; Fink, M.; Lerosey, G. *Nat. Phys.* **2013**, *9*, 55−60.
(2) Yao, J.; Liu, Z.; Liu, Y.; Wang, Y.; Sun, C.; Bartal, G.; Stacy, A. M.; Zhang, X. *Science* **2008**, *321*, 930−930.
(3) Krishnamoorthy, H. N. S.; Jacob, Z.; Narimanov, E.; Kretzschmar, I.; Menon, V. M. *Science* **2012**, *336*, 205−209.
(4) Noginov, M. A.; Li, H.; Barnakov, Y. A.; Dryden, D.; Nataraj, G.; Zhu, G.; Bonner, C. E.; Mayy, M.; Jacob, Z.; Narimanov, E. E. *Opt. Lett.* **2010**, *35*, 1863−1865.
(5) Jacob, Z.; Kim, J. Y.; Naik, G. V.; Boltasseva, A.; Narimanov, E. E.; Shalaev, V. M. *Appl. Phys. B: Laser Opt.* **2010**, *100*, 215−218.
(6) Kauranen, M.; Zayats, A. V. *Nat. Photonics* **2012**, *6*, 737−748.
(7) Poddubny, A.; Irosh, I.; Belov, P.; Kivshar, Y. *Nat. Photonics* **2013**, *7*, 958−967.
(8) Noginov, M. A.; Barnakov, Y. A.; Zhu, G.; Tumkur, T.; Li, H.; Narimanov, E. E. *Appl. Phys. Lett.* **2009**, *94*, 151105.
(9) Custodio, L. M.; Sousa, C. T.; Ventura, J.; Teixeira, J. M.; Marques, P. V. S.; Araujo, J. P. *Phys. Rev. B* **2012**, *85*, 165408.
(10) Pollard, R. J.; Murphy, A.; Hendren, W. R.; Evans, P. R.; Atkinson, R.; Wurtz, G. A.; Zayats, A. V.; Podolskiy, V. A. *Phys. Rev. Lett.* **2009**, *102*, 127405.
(11) Wurtz, G. A.; Pollard, R.; Hendren, W.; Wiederrecht, G. P.; Gosztola, D. J.; Podolskiy, V. A.; Zayats, A. V. *Nat. Nanotechnol.* **2011**, *6*, 106−110.
(12) Kawata, S.; Ono, A.; Verma, P. *Nat. Photonics* **2008**, *2*, 438−442.
(13) Yao, J.; Wang, Y.; Tsai, K.-T.; Liu, Z.; Yin, X.; Bartal, G.; Stacy, A. M.; Wang, Y.-L.; Zhang, X. *Philos. Trans. R. Soc., A* **2011**, *369*, 3434−3446.
(14) Yao, J.; Tsai, K.-T.; Wang, Y.; Liu, Z.; Bartal, G.; Wang, Y.-L.; Zhang, X. *Opt. Express* **2009**, *17*, 22380−22385.
(15) Casse, B. D. F.; Lu, W. T.; Huang, Y. J.; Gultepe, E.; Menon, L.; Sridhar, S. *Appl. Phys. Lett.* **2010**, *96*, 023114.
(16) Belov, P. A.; Palikaras, G. K.; Zhao, Y.; Rahman, A.; Simovski, C. R.; Hao, Y.; Parini, C. *Appl. Phys. Lett.* **2010**, *97*, 191905.
(17) Ginzburg, P.; Rodriguez Fortuno, F. J.; Wurtz, G. A.; Dickson, W.; Murphy, A.; Morgan, F.; Pollard, R. J.; Iorsh, I.; Atrashchenko, A.; Belov, P. A.; Kivshar, Y. S.; Nevet, A.; Ankonina, G.; Orenstein, M.; Zayats, A. V. *Opt. Express* **2013**, *21*, 14907−14917.
(18) Narimanov, E. E.; Li, H.; Barnakov, Y. A.; Tumkur, T. U.; Noginov, M. A. *Opt. Express* **2013**, *21*, 14956−14961.
(19) Kabashin, A. V.; Evans, P.; Pastkovsky, S.; Hendren, W.; Wurtz, G. A.; Atkinson, R.; Pollard, R.; Podolskiy, V. A.; Zayats, A. V. *Nat. Mater.* **2009**, *8*, 867−871.
(20) Soukoulis, C. M.; Linden, S.; Wegener, M. *Science* **2007**, *315*, 47−49.
(21) Soukoulis, C. M.; Wegener, M. *Nat. Photonics* **2011**, *5*, 523−530.
(22) Yakovlev, V. V.; Dickson, W.; Murphy, A.; McPhillips, J.; Pollard, R. J.; Podolskiy, V. A.; Zayats, A. V. *Adv. Mater.* **2013**, *25*, 2351−2356.
(23) Ginzburg, P.; Krasavin, A. V.; Poddubny, A. N.; Belov, P. A.; Kivshar, Y. S.; Zayats, A. V. *Phys. Rev. Lett.* **2013**, *111*, 036804.

(24) Chu, J.-Y.; Wang, T.-J.; Chang, Y.-C.; Lin, M.-W.; Yeh, J.-T.; Wang, J.-K. *Ultramicroscopy* **2008**, *108*, 314−319.
(25) Keilmann, F.; Hillenbrand, R. *Philos. Trans. R. Soc., A* **2004**, *362*, 787−805.
(26) Bek, A.; Vogelgesang, R.; Kern, K. *Rev. Sci. Instrum.* **2006**, *77*, 043703.
(27) Alonso-Gonzalez, P.; Albella, P.; Schnell, M.; Chen, J.; Huth, F.; Garcia-Etxarri, A.; Casanova, F.; Golmar, F.; Arzubiaga, L.; Hueso, L. E.; Aizpurua, J.; Hillenbrand, R. *Nat. Commun.* **2012**, *3*, 684.
(28) Chen, J.; Badioli, M.; Alonso-Gonzalez, P.; Thongrattanasiri, S.; Huth, F.; Osmond, J.; Spasenovic, M.; Centeno, A.; Pesquera, A.; Godignon, P.; Zurutuza Elorza, A.; Camara, N.; Javier Garcia de Abajo, F.; Hillenbrand, R.; Koppens, F. H. L. *Nature* **2012**, *487*, 77−81.
(29) Cheng, T.-Y.; Wang, H.-H.; Chang, S. H.; Chu, J.-Y.; Lee, J.-H.; Wang, Y.-L.; Wang, J.-K. *Phys. Chem. Chem. Phys.* **2013**, *15*, 4275−4282.
(30) Zentgraf, T.; Dorfmueller, J.; Rockstuhl, C.; Etrich, C.; Vogelgesang, R.; Kern, K.; Pertsch, T.; Lederer, F.; Giessen, H. *Opt. Lett.* **2008**, *33*, 848−850.
(31) Alonso-Gonzalez, P.; Schnell, M.; Sarriugarte, P.; Sobhani, H.; Wu, C.; Arju, N.; Khanikaev, A.; Golmar, F.; Albella, P.; Arzubiaga, L.; Casanova, F.; Hueso, L. E.; Nordlander, P.; Shvets, G.; Hillenbrand, R. *Nano Lett.* **2011**, *11*, 3922−3926.
(32) Dorfmueller, J.; Dregely, D.; Esslinger, M.; Khunsin, W.; Vogelgesang, R.; Kern, K.; Giessen, H. *Nano Lett.* **2011**, *11*, 2819−2824.
(33) Elser, J.; Wangberg, R.; Podolskiy, V. A.; Narimanov, E. E. *Appl. Phys. Lett.* **2006**, *89*, 261102.
(34) Evans, P. R.; Kullock, R.; Hendren, W. R.; Atkinson, R.; Pollard, R. J.; Eng, L. M. *Adv. Funct. Mater.* **2008**, *18*, 1075−1079.
(35) Schnell, M.; Garcia-Etxarri, A.; Huber, A. J.; Crozier, K. B.; Borisov, A.; Aizpurua, J.; Hillenbrand, R. *J. Phys. Chem. C* **2010**, *114*, 7341−7345.
(36) Wells, B. M.; Zayats, A. V.; Podolskiy, V. A. *Phys. Rev. B* **2014**, *89*, 035111.